[6] For other catalytic applications of ligand **1** see: a) C. Bolm, K. Muñiz-Fernandez, A. Seger, G. Raabe, *Synlett* **1997**, 1051; b) C. Bolm, K. Muñiz-Fernandez, A. Seger, G. Raabe, K. Günther, *J. Org. Chem.* **1998**, *63*, 7860; c) C. Bolm, K. Muñiz, J. P. Hildebrand, *Org. Lett.* **1999**, *1*, 491; d) K. Muñiz, PhD thesis, RWTH Aachen, **1998**; e) see also in: K. Muñiz, C. Bolm, *Chem. Eur. J.* **2000**, *6*, 2309.

[7] a) C. Bolm, K. Muñiz, *Chem. Commun.* **1999**, 1295; b) C. Bolm, N. Hermanns, J. P. Hildebrand, K. Muñiz, *Angew. Chem.* **2000**, *112*, 3607; *Angew. Chem. Int. Ed.* **2000**, *39*, 3465.

[8] Use of 1-[*o*-(diphenylhydroxymethyl)-phenyl]-3-*tert*-butyloxazoline in the addition of the phenylzinc species to 4-chlorobenzaldehyde resulted in an *ee* of 62% compared with 97% obtained with ferrocene **1**.

[9] A positive effect upon the introduction of a metal fragment on the enantioselectivity in the Pd-catalyzed asymmetric allylations was found by Helmchen et al. There, a P,N-chelating ligand with a cymantrene unit was used. a) G. Helmchen, S. Kudis, P. Sennhenn, H. Steinhagen, *Pure Appl. Chem.* **1997**, *69*, 513; b) S. Kudis, G. Helmchen, *Angew. Chem.* **1998**, *110*, 3210; *Angew. Chem. Int. Ed.* **1998**, *37*, 3047. Studies on the use of the manganese tricarbonyl complex of **2** (M = [Mn(CO)$_3$]) in the catalyzed phenyl transfer revealed a slightly lower enantioselectivity compared to that of **3** (97% *ee* in the addition onto 4-chlorobenzaldehyde). The complete results of our screening study of metal complexes will be reported in due course.

[10] For other catalyzed diphenylzinc additions to aldehydes, see: a) P. I. Dosa, J. C. Ruble, G. C. Fu, *J. Org. Chem.* **1997**, *62*, 444; b) W.-S. Huang, Q.-S. Hu, L. Pu, *J. Org. Chem.* **1999**, *64*, 7940; c) W.-S. Huang, L. Pu, *Tetrahedron Lett.* **2000**, *41*, 145, and references therein.

[11] W. H. Bosch, U. Englert, B. Pfister, R. Stauber, A. Salzer, *J. Organomet. Chem.* **1996**, *506*, 273.

[12] Some compounds containing this moiety have been used for labeling of biologically active substances because of the importance of radioactive rhenium isotopes for medicinal diagnosis and treatment. For an example see: S. Top, H. El Hafa, A. Vessières, J. Quivy, J. Vaissermann, D. W. Hughes, M. J. McGlinchey, J.-P. Mornon, E. Thoreau, G. Jaouen, *J. Am. Chem. Soc.* **1995**, *117*, 8372.

[13] S. Top, J.-S. Lehn, P. Morel, G. Jaouen, *J. Organomet. Chem.* **1999**, *583*, 63.

[14] New compounds have been fully characterized by spectroscopic methods and elemental composition established by combustion analysis or HR-MS (see Supporting Information). A concise comparison between complexes **1** and **3** will be discussed elsewhere.

[15] R. Appel, *Angew. Chem.* **1975**, *87*, 863; *Angew. Chem. Int. Ed. Engl.* **1975**, *14*, 801.

[16] a) V. Snieckus, *Chem. Rev.* **1990**, *90*, 879; concerning the analogous lithiation of ferrocenyl oxazolines, see: b) T. Sammakia, H. A. Latham, D. R. Schaad, *J. Org. Chem.* **1995**, *60*, 10; c) Y. Nishibayashi, S. Uemura, *Synlett* **1995**, 79; d) C. J. Richards, A. W. Mulvaney, *Tetrahedron: Asymmetry* **1996**, *7*, 1419.

[17] Attempted *ortho*-metalation of **6** with *s*BuLi resulted in the formation of products which presumably stem from nucleophilic addition. Those reactions are well-known from the chemistry of chromium(tricarbonyl) arene complexes. For examples, see: E. P. Kündig, D. Amurrio, R. Liu, A. Ripa, *Synlett* **1991**, 657.

[18] For the nomenclature, see: K. Schlögl, *Top. Stereochem.* **1967**, *1*, 39.

[19] Crystal data for **3**: trigonal, $a = 11.1669(3)$, $c = 35.5114(14)$ Å, $Z = 2 \times 3$ (two symmetrically independent molecules), $V = 3835.0(3)$ Å^3, space group $P3_2$, colorless crystals obtained by recrystallization from MTBE, measured on a SMART Bruker diffractometer at 100 K, $R = 0.046$, $R_w = 0.033$, GOF = 1.471. Crystallographic data (excluding structure factors) for the structure reported in this paper have been deposited with the Cambridge Crystallographic Data Centre as supplementary publication no. CCDC-147702. Copies of the data can be obtained free of charge on application to CCDC, 12 Union Road, Cambridge CB2 1EZ, UK (fax: (+44) 1223-336-033; e-mail: deposit@ccdc.cam.ac.uk).

[20] In the analogous dialkylzinc additions to aldehydes this background reaction takes place only to a minor extent. For reviews on this reaction, see: a) R. Noyori, M. Kitamura, *Angew. Chem.* **1991**, *103*, 34; *Angew. Chem. Int. Ed. Engl.* **1991**, *30*, 49; b) K. Soai, S. Niwa, *Chem. Rev.* **1992**, *92*, 833; c) see also: K. Soai, T. Shibata in *Comprehensive Asymmetric Catalysis*, *Vol. 2* (Eds.: E. N. Jacobsen, A. Pfaltz, H. Yamamoto), Springer, Berlin, **1999**, p. 911.

[21] In a separate study (ref. [6c]), we had shown that the use of diastereomeric mixtures of **1** can lead to high enantioselectivity. As a consequence we proposed that this phenomenon could be exploited in cases where the directed *ortho*-metalation was not completely diastereoselective. Here we have now found that using 10 mol% of a 7:1 mixture of (S,R_p)-**3** and diastereomeric (S,S_p)-**3**, the phenylation of *p*-chlorobenzaldehyde proceeded with 97% *ee*. Thus, it appears that this mixture as such can be used in catalysis. The overall process applying **3** in the aryl transfer is thereby simplified even further.

Individual Alumina Nanotubes**

Lin Pu,* Ximao Bao, Jianping Zou, and Duan Feng

Avid attention has been given to the preparation, properties, and applications of nanotubes of different materials. Nanotubes composed of carbon,[1] tungsten disulfide (WS_2),[2] boron nitride (BN),[3] vanadium oxide [$VO_{2.40}(C_{16}H_{33}NH_2)$],[4] titanium dioxide ($TiO_2$),[5] and others, were studied during the last decade. However, the reproducible usage of nanotubes in electrical devices is complicated by the fact that the tubes exist in different chiralities and diameters.[6] Moreover, the raw materials consist of dense networks of closely connected nanotubes, and individual tubes are often obtained by ultrasonic agitation, which may introduce defects into the tubes.[7] Here we report on two easy and controlled electrochemical-anodizing routes for the synthesis of individual alumina nanotubes (ANTs) in a single fabricating step. The structure of ANTs provides clues to unraveling the mechanism of nanotube growth and gives valuable hints on solving the long-standing problem of the self-organization mechanism in the porous anodization of aluminum.[8–15]

Two different preparation methods (Figure 1), designated normal stepwise anodization (NSA) and lateral stepwise anodization (LSA), were used to make ANTs. The major difference between these two arrangements is the position on the sample (Al/Si) to which the potential difference U is applied. For NSA, it is the bottom surface of the Si substrate, and for LSA, the top surface of the Al metal film. This results in completely different current paths for the two methods. Note, however, that the orientation of the sample is not important.

The transmission electron microscope (TEM) images in Figure 2 show a general view of the ANTs. They are attached to the anodic porous alumina (APA) mother film. In the TEM

[*] Dr. L. Pu, Prof. Dr. X. Bao, Dr. J. Zou, Prof. Dr. D. Feng
National Laboratory of Solid State Microstructures
and
Department of Physics, Nanjing University
Nanjing 210093 (China)
Fax: (+86) 25-359-5535
E-mail: xmbao@nju.edu.cn

[**] This work was supported by the National Natural Science Foundation under the contract No. 59832100.

  0044-8249/01/11308-1538 $ 17.50+.50/0

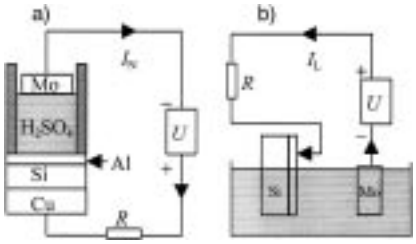

Figure 1. Sketch of preparation methods for ANTs. For details see the Experimental Section. a) NSA: After 360 s of anodization, power was turned off for 60 s, then anodizing was carried out again for 173 s. Al was almost completely oxidized after about 100 s. b) LSA: After open-circuit dissolution for 120 s, the sample was anodized for 292 s. $R = 16.9\ \Omega$. The time depends on fabrication conditions such as the thickness of the Al film, the temperature, concentration and species of the electrolyte, and the resistance of the Al/Si interface.

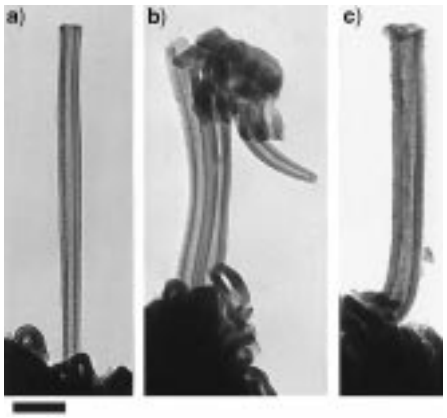

Figure 2. TEM morphologies of the ANTs. a), b) NSA tubes, c) LSA tubes. Scale bar: 100 nm.

studies, the sample holder could be tilted at angles of -30, 0, and $+30^\circ$ without changing the dimensions and contrast of the products; hence, they are tubelike in shape. The longest ANT observed was 650 nm in length and had outer and inner diameters of 35 and 12 nm (Figure 2a). Some bundles of ANTs (Figure 2b) were also present. The ANTs fabricated by the two methods have the same structure and differ only in size: the NSA tubes are smaller than the LSA tubes. The main factor determining the tube size is whether or not the current path of the growth method passes through the interface region.

The ANTs often appeared in the cleavage regions of the APA films. Figure 3 shows three typical cleavages of the films, with fracture morphologies that resemle a spider web, a screw thread, and concentric circles. The cleavages presumably correspond to high tensile stress in the thin APA film at zero electric field.[16] The measured strain at failure of the film can be as high as 0.13 (13% change in volume) for NSA samples (Figures 3a and 3b) and around 0.10 for LSA samples (Figure 3c). Although the precise mechanism of these kinds of cleavage is unclear, we assume that they are related to tube formation.

Detailed images of the cleavages are presented in Figure 4, and the cellular structure of the APA film is shown in Figure 5. In the classical model of the cellular structure of APA films[8, 10, 11] (Figure 5b), the cells are separated by nominal

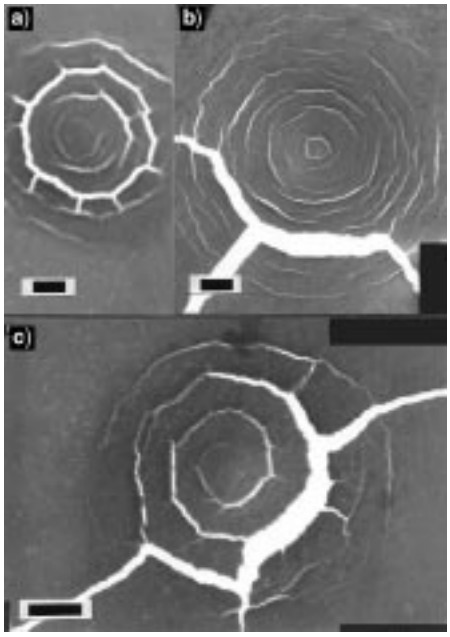

Figure 3. TEM morphologies of cleavage regions within the APA film. The fracture morphology resembles a spider web (a; NSA samples), a screw thread (b; NSA samples), or concentric circles (c; LSA samples). The ANTs often appeared in these regions. Scale bars: 2 μm.

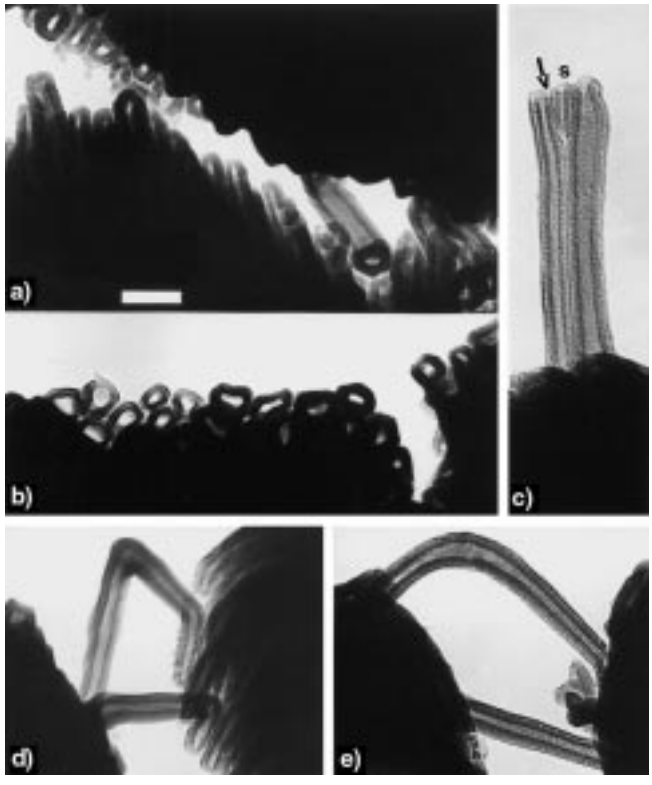

Figure 4. Detailed TEM images of the cleavage regions reveal that the ANTs are completely detached cells of the APA film (NSA samples). a) Three incompletely detached cells of the film (right-hand side of the image). b) The cleavages occurred along the cell boundary (top view). c) A short stagnant cell (marked by S) in the middle of a bundle of cells. A void underlies this cell, and cracks (indicated by an arrow) are evident along the cell boundaries. d) A bent cell. e) The image of the sample shown in Figure 4d taken after tilting the TEM sample holder at various angles reveals that the cell can be bent at an angle of nearly 90° without any observable cracking. All images have the same scale. Scale bar: 100 nm.

  0044-8249/01/11308-1539 $ 17.50+.50/0

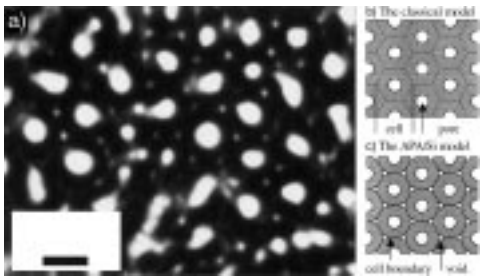

Figure 5. a) A bottom-view TEM image of the APA film reveals voids located at the junctions of three cell boundaries (LSA samples). b) Classical model of the cellular structure of an APA film. c) Refined model of the cellular structure of APA/Si, with small voids at the junctions of three cell boundaries. Scale bar: 50 nm.

boundaries (dotted lines) and arranged in a hexagonal configuration. Figures 4a and 4b reveal that the film cleavage evidently occurred along cell boundaries.[13, 17] The right-hand side of Figure 4a shows three incompletely detached cells of the APA film. Both ends of the tubes are attached to the mother film. Figure 4d reveals clearly a tube whose closed tip is attached to the film. Figure 4e shows that an ANT can be bent at an angle of nearly 90° without any observable cracking. This good elasticity should be helpful in obtaining long, crack-free tubes.

Films anodized for a short time contain many stagnant cells which grew slowly or ceased to grow during anodization.[8, 12] Such a cell can be seen in Figure 2b (the short tube with a closed tip on the right), and Figure 4c shows a stagnant cell S in a tube bundle. In TEM studies, we found that the region immediately underlying the cell S is completely transparent to the electron beam, that is, it is empty. We refer to it as a void and deduce that it already existed before the bundle detached from the mother film.

In addition to this void, another kind of void is often observed at the junctions of the cell boundaries (Figure 5a). Their formation mechanism might be the same as that of the defect reported by Macdonald.[18] The refined model of an APA film based on this finding is shown in Figure 5c. It shows cell boundaries and voids located at the junctions of three neighboring cells. We may further postulate that this cellular structure is actually an incipient close-packed bundle of alumina nanotubes. Cell-boundary regions containing structural defects such as voids and cracks should provide easy paths for film cleavage, and therefore voids and the detachment of cells may be detected. Furthermore, since all observed tubes are shorter than the film thickness (around 800 nm), and incomplete detachment of cells was detected, we deduce that individual ANTs are completely detached cells of the APA film.

In contrast to conventional constant-voltage anodized films,[10, 13] the APA/Si films fabricated by stepwise methods have a highly disordered structure. This disorder may be an important reason for the development of tubes. For NSA, when growing ends of the cells have not proceeded to the interface, the potential drop across the barrier layer should decrease slightly due to interruption of film growth by switching the power on and off and the slight temperature rise in the electrolyte (0.4–0.6°C in our case without agitation). These effects may cause local irregularities of the cell structure, such as stagnation, branching, merging, and inhomogeneous variation in cell diameters. Therefore, a higher local tensile stress may develop within the film. Figure 6 shows a side view of the mother film of ANTs. Evidently, the growing end of the cell is dominated by the

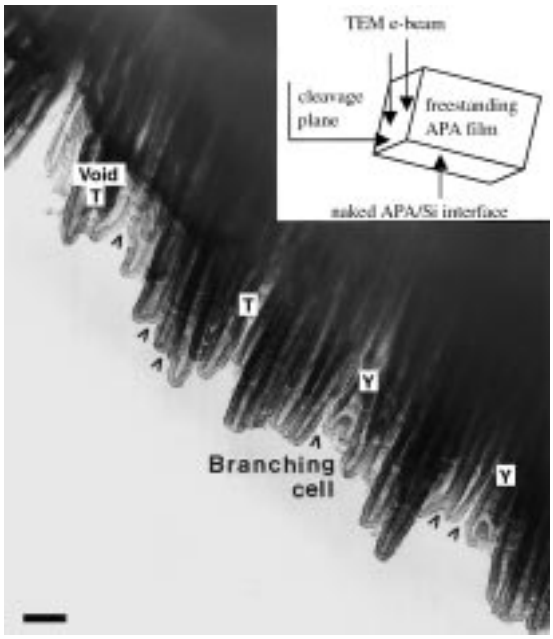

Figure 6. A side-view TEM image of the cleavage plane of the APA film (NSA samples) reveals the detailed morphology of the near-interface region. For details see text. The inset depicts the imaging arrangement. Scale bar: 100 nm.

irregularity. Except for two Y-shaped branched cells, most of the cells are truncated in a conelike or flat-headed manner. A tendency for branching is evident, as is a progressively diminishing cell diameter, which is presumably mainly due to the effect of the interface (see below). The cracks visible at the cell boundaries of these branching cells (indicated by V-shaped arrows) should provide easy paths for cell detachment. Figure 6 also shows some voids (indicated by T) within the cell-boundary region. The voids may decrease the strength of these regions, so that the thin APA film can cleave easily along the cell boundaries.

Besides the temperature, the Al/Si interface should exert a dominant effect on disordered cell growth and is thus important for the development of tubes. Because of considerable misfit within the interface region between the APA film and Si after the polycrystalline Al film is almost completely oxidized, the APA film may be easily detached from the Si substrate. Under the influence of tensile stress, thin free-standing film curls, so it cleaves easily and then develops detached cells. Furthermore, the interface can induce a nonuniform growth of the APA film in the near-interface region. Cell branching within the near-interface region (Figure 6) could be attributable to the effect of the interface (Figure 7). Because the cell size is proportional to the forming voltage U_C, when the interface induces a decrease in the potential drop across the barrier layer of the cell, the

  0044-8249/01/11308-1540 $ 17.50+.50/0

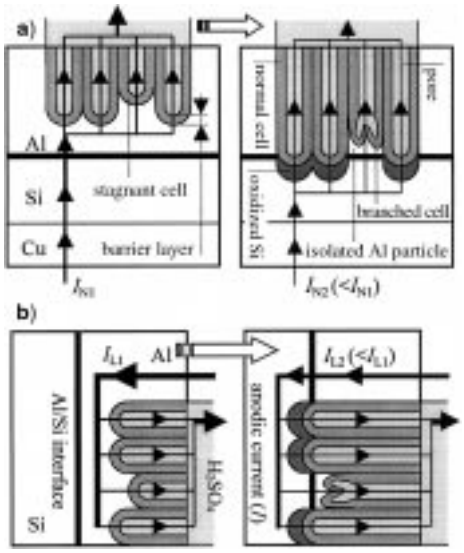

Figure 7. Schematic diagram of the effect of the substrate on the development of tubes. For details see text and the Experimental Section. a) NSA: $I_{N1} \approx U/(R_B + R_I)$, $U_{CN1} \approx I_{N1}R_B$ (left); $I_{N2} \approx U/(R_B + R_O)$, $U_{CN2} \approx I_{N2}R_B$ (right). Note that $R_I < R_O$, since the Al/Si interface consisting of native oxide is thinner than the oxidized Si layer after anodization ($I_{N1} > I_{N2}$); hence, $U_{CN1} > U_{CN2}$. b) LSA: $I_{L1} \approx U/R_B$, $U_{CL1} \approx I_{L1}R_B$ (left); $I_{L2} \approx U/(R_B + R_O)$, $U_{CL2} \approx I_{L2}R_B$ (right). From $I_{L1} > I_{L2}$ follows $U_{CL1} > U_{CL2}$.

cell will branch.[10, 11] Nevertheless, the decrement of the forming voltage should be mainly due to the sudden increase in the electrical resistance of the anodizing circuit during this period. Additionally, slightly diminishing cell diameters near the growing ends could be due to high thermal resistance of the thin film and the interface.

The Y-shaped branched cells may be derived from stagnant cells (Figure 7). For example, in NSA samples, the thicknesses of the Al/Si interface (d_I), the oxidized Si layer (d_O), and the barrier layer (d_B) are about 4, 10, and 10 nm, respectively. In a rough estimation, it is reasonable to assume that the resistances of the Al/Si interface (R_I), the oxidized Si layer (R_O), and the barrier layer are proportional to their thicknesses. For the NSA sample (Figure 7a), the reducing ratio of the forming voltage is: $U_{CN2}/U_{CN1} \approx (R_B + R_I)/(R_B + R_O) \approx (d_B + d_I)/(d_B + d_O) \approx 1/\sqrt{2}$. Because the cell diameter is proportional to the potential drop U_C across the barrier layer of the cell, reducing the voltage by a factor of $1/\sqrt{2}$ results in the appearance of twice as many cells to maintain the original total area of the APA film, and most cells would branch into two cells of smaller diameter (Y-shaped branched cells). Under the influence of the interface, only these stagnant cells would branch dominantly until the power is turned off, because the isolated Al particles underlying the stagnant cells can sustain their continuous growth and branching. The other, normal cells, whose growing ends have already connected with or slightly penetrated into the interface region, will cease to grow at this moment. Note that the density of the stagnant cells is related to the density of the Al grain boundaries in the pre-anodized polycrystalline Al film. The branching certainly induced the highly local irregularity of the cell structure, as well as the increased stress of the APA film. It should be beneficial for the detachment of the film from the substrate and for the separation of the cells from each other along the cell boundaries.

In conclusion, we have presented two methods for the controlled fabrication of ANTs and deduced that they are completely detached cells of the APA film. The semiconductor substrate exerts a dominant effect on the detachment of cells. This study may open fascinating possibilities for further chemical and physical explorations of nanostructures such as nanowires, cylindrical capacitors, MOSFETs, and containers.

Experimental Section

Preparation of the ANTs (see Figure 1): An electron beam evaporated 400 nm thick Al (99.99%) film on a p-type, 0.5 Ω cm, 5°-off ⟨100⟩ Si substrate (Al/Si) was anodized in dilute sulfuric acid (15 wt%). The potential difference U was 40 V dc. Before anodizing, the temperature of the electrolyte was (10.0 ± 0.2) °C. Anodization was continued until the APA film detached from the substrate. Then the free-standing film was cleaned in flowing distilled water for a prolonged period of time. After that, it was transferred to copper TEM grids and stored in a dry tube at room temperature. The specimens were directly examined with JEM-200CX and JEM-2000EX transmission electron microscopes operated at 120 kV.

Effect of the substrate on the development of tubes (see Figure 7): Since the resistances of the Al/Si interface(R_I), the barrier layer (R_B), and the oxidized Si layer (R_O) are rather large, those of the electrolyte, the series resistor ($R = 16.9\ \Omega$), low-resistivity p-type Si, and Al metal can be neglected. The power voltage U is 40 V dc, and it is the forming voltage of the cell U_C, that is, the potential drop IR_B across the barrier layer, that largely determines the cell size. The difference in cell size of the two methods results from $U_{CL1} > U_{CN1}$, which is due to the interface. Formation of the Y-branched cells is also due to the interface.

Received: July 19, 2000
Revised: December 27, 2000 [Z15485]

[1] S. Iijima, *Nature* **1991**, *354*, 56–58.
[2] R. Tenne, L. Margulius, M. Genut, G. Hodes, *Nature* **1992**, *360*, 444–446.
[3] N. G. Chopra, R. J. Luyken, K. Cherrey, V. H. Crespi, M. L. Cohen, S. G. Louie, A. Zettl, *Science* **1995**, *269*, 966–967.
[4] M. E. Spahr, P. Bitterli, R. Nesper, M. Müller, F. Krumeich, H. U. Nissen, *Angew. Chem.* **1998**, *110*, 1339–1342; *Angew. Chem. Int. Ed.* **1998**, *37*, 1263–1265.
[5] T. Kasuga, M. Hiramatsu, A. Hoson, T. Sekino, K. Niihara, *Langmuir* **1998**, *14*, 3160–3163.
[6] R. Satio, G. Dresselhaus, M. S. Dresselhaus, *Physical Properties of Carbon Nanotubes*, Imperial College Press, London, **1998**.
[7] G. T. Kim, J. Muster, V. Krstic, J. G. Park, Y. W. Park, S. Roth, M. Burghard, *Appl. Phys. Lett.* **2000**, *76*, 1875–1877.
[8] F. Keller, M. S. Hunter, D. L. Robinson, *J. Electrochem. Soc.* **1953**, *100*, 411–419.
[9] T. P. Hoar, J. Yahalom, *J. Electrochem. Soc.* **1963**, *110*, 614–621.
[10] J. W. Diggle, T. C. Downie, C. W. Goulding, *Chem. Rev.* **1969**, *69*, 365–405.
[11] J. P. O'Sullivan, G. C. Wood, *Proc. R. Soc. London A* **1970**, *317*, 511–543.
[12] R. C. Furneaux, W. R. Righy, A. P. Davidson, *Nature* **1989**, *337*, 147–149.
[13] H. Masuda, F. Hasegwa, S. Ono, *J. Electrochem. Soc.* **1997**, *144*, L127–L130.
[14] O. Jessensky, F. Müller, U. Gösele, *Appl. Phys. Lett.* **1998**, *72*, 1173–1175.
[15] F. Y. Li, L. Zhang, R. M. Metzger, *Chem. Mater.* **1998**, *10*, 2470–2480.
[16] D. A. Vermilyea, *J. Electrochem. Soc.* **1963**, *110*, 345–346.
[17] K. Wada, T. Shimohira, M. Yamada, N. Baba, *J. Mater. Sci.* **1986**, *21*, 3810–3816.
[18] D. D. Macdonald, *J. Electrochem. Soc.* **1993**, *140*, L27–L30, and references therein.

  0044-8249/01/11308-1541 $ 17.50+.50/0